Micelles

DOI: 10.1002/ange.201002551

Self-Division of Macroscopic Droplets: Partitioning of Nanosized Cargo into Nanoscale Micelles**

*Kevin P. Browne, David A. Walker, Kyle J. M. Bishop, and Bartosz A. Grzybowski**

Reactions that produce surface-active compounds at the liquid–liquid interface can divide large droplets into smaller ones (Figure 1). This effect of "autopoietic" self-reproduction was originally studied by Luisi and co-workers[1,2] in the context of self-dividing micelles and inverse micelles. This pioneering work was based on two-phase (oil–water) systems, in which surfactants were created at the liquid–liquid interface by either basic hydrolysis of esters or anhydrides in the oil phase by hydroxide ions in the aqueous phase,[1] or by long-chain alcohol oxidation at the liquid–liquid interface by permanganate ions in the aqueous phase.[2] Later work by Luisi and co-workers[3,4] and also by Szostak and co-workers[5,6] demonstrated self-reproduction in more intricate bilayer and even multilamellar[6] vesicles. Such fatty acid vesicles can serve as artificial "reactors" that support the replication of nucleic acids.[4] Despite these exciting results, control over the ultimate sizes of the dividing micelles remains limited and little is known about the stability (both kinetic and thermodynamic) of the "daughter" entities. Herein we show that a self-division process can be propagated from macroscopic emulsion droplets all the way down to nanoscopic micelles (or inverse micelles), the sizes of which are controlled by the pH of the solution. In addition to these thermodynamically stable phases, the system also features a kinetically stable microemulsion phase that is observed when the pH is lowered below a certain critical value. The existence and stabilities of these phases as well as the hysteretic behavior of the system upon pH changes are explained by a theoretical model that accounts for the chemical, curvature, and electrostatic contributions to the interfacial surface free energy of the droplets. Controllable macro-to-nano division allows the partitioning of cargo (here, nanoscopic particles) originally contained in a macroscopic drop into the "progeny" nanomicelles with a precision as low as one or two particles per micelle. This method can open new perspectives for the engineering of emulsions with well-defined macromolecular or nanoscopic contents.

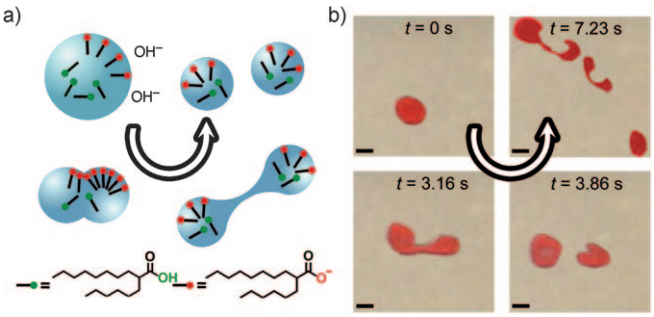

Figure 1. a) An interfacial reaction drives the spontaneous (i.e., without any agitation) division of large droplets (here, 100 mL dichloromethane that contains 45% v/v 2-HDA and is suspended in pH 12 KOH solution) into progressively smaller progenies. b) Images of the first few seconds of the division process. Emulsification into nanoscale droplets is complete within 30–60 s. The droplets are dyed with Calco Oil Red for better visualization. Scale bars: 2.5 mm.

The process of droplet division is illustrated in Figure 1 (see also Movie 1 in the Supporting Information). A drop of dichloromethane (typically 80–100 μL) that contains 45–50% (v/v) 2-hexyldecanoic acid (2-HDA) and a small amount (ca. 5 mg mL^{-1}) of Calco Oil Red dye for visualization is placed in a petri dish filled with an aqueous solution of KOH (pH 12). 2-HDA was chosen because it accumulates at the DCM/water interface in its deprotonated form and can thus act as a surfactant. As the interfacial reaction between 2-HDA and the base progresses, more of the deprotonated 2-HDA accumulates at the interface to result in an increase in the interfacial area[7–9] (i.e., the drop "elongates") until the drop divides into smaller, usually two, progenies. These droplets then divide again, and the process continues until the droplets reach nanoscopic dimensions (e.g., $d \approx 30$ nm at pH ≈ 12; see Figure 2).

The ultimate droplet or micelle size d depends on the pH of the basic solution. We studied this dependence by means of dynamic light scattering (DLS). The results summarized in Figure 2 show that for pH values less than approximately 10, the droplets do not divide and the value of d remains approximately constant. At a critical pH value of approximately 10, however, a sharp transition into nanoscopic

[*] K. P. Browne,[+] D. A. Walker,[+] Dr. K. J. M. Bishop, Prof. B. A. Grzybowski
Department of Chemical and Biological Engineering
Northwestern University
2145 Sheridan Rd., Evanston, IL 60208 (USA)
Fax: (+1) 847-491-3728
E-mail: grzybor@northwestern.edu
Homepage: http://dysa.northwestern.edu/
Prof. B. A. Grzybowski
Department of Chemistry
Northwestern University
2145 Sheridan Rd., Evanston, IL 60208 (USA)
[+] These authors contributed equally to this work.

[**] This work was supported by the Non-equilibrium Energy Research Center (NERC) which is an Energy Frontier Research Center funded by the U.S. Department of Energy, Office of Science, Office of Basic Energy Sciences under Award Number DE-SC0000989 (K.P.B., D.A.W., K.J.M.B., B.A.G.).

Supporting information for this article is available on the WWW under http://dx.doi.org/10.1002/anie.201002551.

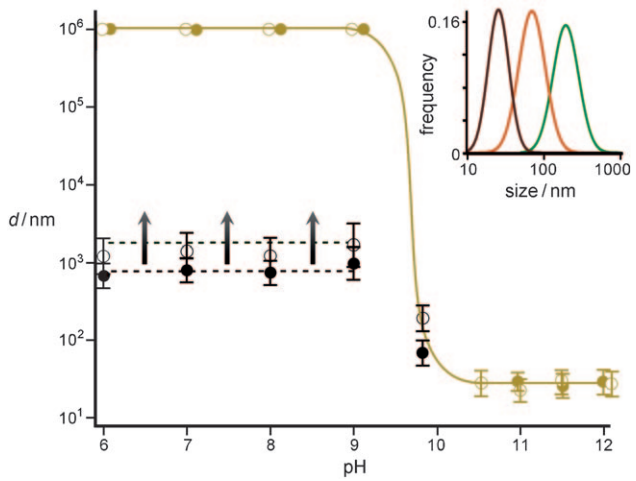

Figure 2. Thermodynamic and kinetic phases of the DCM/2-HDA// KOH droplet system. Macroscopic droplets divide into nanoemulsions above pH ≈ 10. For pH > 10, the nanoemulsion phase is thermodynamically stable (filled brown circles: after 24 h, open brown circles: after 48 h). When the pH is lowered, the droplets become metastable (filled black circles: after 24 h, open black circles: after 48 h) and their size increases with time. Data points for pH > pK_a are shown. For pH < pK_a, coalescence occurs within tens of seconds to minutes. Diameters were determined by DLS. Error bars denote 68% confidence intervals for the droplet diameter centered on the median of the distribution (for details, see the Supporting Information) and are based on at least three measurements for each condition. The inset shows examples of the droplet size distributions (measured by DLS; brown: pH 12.1; orange: pH 9.8 after 24 h; green: pH 9.8 after 48 h). For pH 9.8 at the boundary of the thermodynamically stable region, the droplet size increases with time. For pH 12.1, the $d \approx 30$ nm droplets are stable.

droplets ($d \approx 30$ nm) takes place. In this regime, the droplet size does not change with time, thus indicating that the created nanoemulsions are thermodynamically stable. In addition, however, a kinetically stable (metastable) microemulsion phase can be realized (open and filled black circles in Figure 2) when the pH is lowered from above to below pH 10. Here, the droplet size increases to approximately 1 μm within the first 24 hours from the pH change and the full phase separation ensues within 5–10 days (this process, however, can be accelerated to minutes if pH < pK_a and the electrostatic repulsions that stabilize the emulsion are eliminated).

To explain the process of droplet division, a spherical DCM droplet of the radius R that contains 2-HDA is considered, which, depending on the pH of the surrounding solution, can be either protonated (charge-neutral) or deprotonated (negatively charged). Both forms of 2-HDA are surface active,[10] so that the surface of the drop is covered completely with carboxylic acid groups at a certain surface density Γ (here, $\Gamma \approx 1$ nm^{-2} corresponds to a head group area of ca. 1 nm^2 [11]). The interfacial free energy of the droplet-water interface is approximated as the sum of "chemical" and electrostatic contributions,[12] $\gamma = \gamma_{ch} + \gamma_{es}$. For a flat interface, the chemical contribution to the surface energy of the interface, in the absence of electrostatic effects, is assumed to be constant (γ_o; typically, $\gamma_o \approx 10$ mN m^{-1} for interfaces of water and aliphatic carboxylic acids[15]). Additionally, there is an unfavorable energetic contribution associated with the bending of the interface which is proportional to the square of the curvature for spherical drops, $\gamma_b = {}^1/_2\, k_b/R^2$, where the bending modulus k_b is of the order of 10^{-20} to 10^{-19}.[11] While the bending contribution is negligible for macroscopic droplets (e.g., $\gamma_b \approx 10^{-5}$ mN m^{-1} for micrometer-scale drops), it can be significant for smaller ones (e.g., $\gamma_b \approx 10$ mN m^{-1} for nanometer-sized droplets). Overall, the chemical contribution to the interfacial free energy is approximated by $\gamma_{ch} = \gamma_0 + k_b/2\,R^2$.

To determine the additional electrostatic component of the surface energy, we adopted the so-called charge regulation model, originally conceptualized by Träuble and Eibl[16] and later solidified in the work of Chan and Mitchell,[17] in which the surface charge density σ is related to the surface potential ϕ_s by Equation (1):

$$\sigma = \frac{-e\Gamma K_a}{K_a + [H^+]\exp(-e\varphi_s/k_B T)} \tag{1}$$

where e is the fundamental charge, $K_a = 10^{-pK_a}$ is the acid dissociation constant (p$K_a \approx 5$ for carboxylic acids), $[H^+] = 10^{-pH}$ is the H^+ ion concentration, and $k_B T$ is the thermal energy. Additionally, the surface charge is related to the surface potential through the (linearized) Poisson–Boltzmann (PB) equation, $\nabla^2\phi = \kappa^2\phi$ with $\kappa = (2c_s e^2/\varepsilon_0 \varepsilon k_B T)^{1/2}$, where κ^{-1} is the screening length, c_s is the salt concentration (in the absence of additional electrolytes, $c_s = 10^{-(14-pH)}$ for basic conditions and $c_s = 10^{-pH}$ for acidic conditions), and $\varepsilon_0\varepsilon$ is the dielectric permittivity of the aqueous phase (i.e., $\varepsilon \approx 80$). Solving the PB equation and using the electrostatic relation, $\sigma = -\varepsilon_0\varepsilon(d\phi/dr)_R$, gives the linear relation between σ and ϕ_s, $\sigma = \varepsilon_0\varepsilon(1+\kappa R)\phi_s/R$. Since the latter equation has to be satisfied also at equilibrium, its combination with Equation (1) results in Equation (2):

$$\frac{\varphi_s \varepsilon_0 \varepsilon(1+\kappa R)}{R} = \frac{-e\Gamma K_a}{K_a + [H^+]\exp(-e\varphi_s/k_B T)} \tag{2}$$

This nonlinear equation may be solved numerically to give the surface potential, ϕ_s, as well as the fraction of dissociated groups at equilibrium, $\theta = |\sigma|/e\Gamma$. The dissociation of some of the carboxylic groups (i.e., because of the electrostatic contributions) results in the free energy per unit area γ_{es} to be given by $\gamma_{es} = \sigma\phi_s/2 + k_B T\Gamma \ln(1-\theta)$ with respect to a reference state in which all carboxylic groups are protonated (see reference [17] for the derivation).

We can now estimate the change in the total interfacial free energy ΔF starting from the reference state of one drop of radius R_0 and breaking up into N smaller drops, each of radius R, $\Delta F = N4\pi R^2\gamma\ (R) - 4\pi R_0^2\gamma\ (R_0)$. Because the total volume of the droplets is conserved, $N = (R_0/R)^3$ and $\Delta F = 4\pi R_0^2[R_0\gamma(R)/R - \gamma(R_0)]$. This function is plotted in Figure 3a for various pH conditions and experimental values of the surfactant pK_a, surface density Γ, temperature, and dielectric constant ε. Below a critical pH value of approximately 10, the large drop is thermodynamically stable—that is, ΔF is minimal for $N = 1$. As the pH is increased, however, it

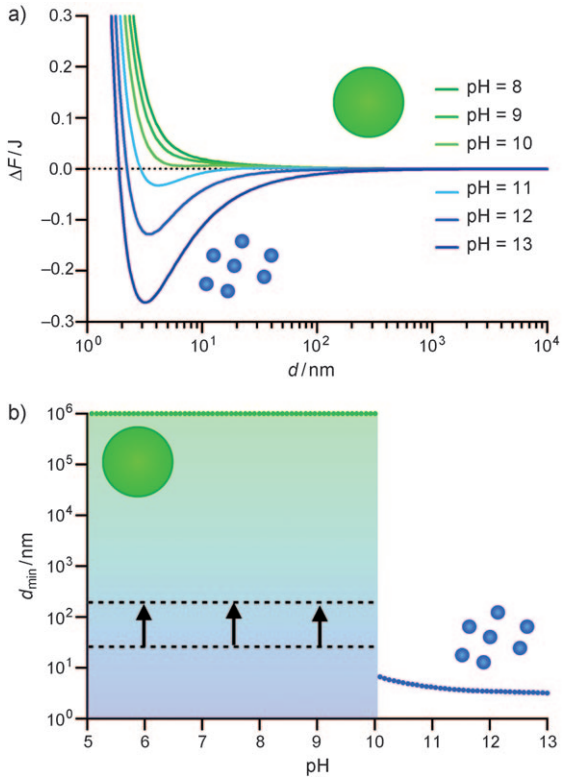

Figure 3. Results of the theoretical model. a) Difference in the total interfacial free energy ΔF upon drop break-up for pH values that range from 8 to 13. The initial state consists of a single droplet of the diameter $d_0 = 1$ mm; the final state consists of N identical droplets of size d. For pH values less than ca. 10, the initial state is thermodynamically favorable; however, for pH values greater than ca. 10, nanoscale droplets form because of the electrostatic repulsion between the charged head groups of the surfactants. b) Droplet size for the minimum free energy configuration as a function of pH. The shaded region denotes a metastable regime, in which small droplets originally created at high pH values aggregate and phase separate. The chemical contribution to the surface energy is $\gamma_o = 10\ \mathrm{mN\,m^{-1}}$, and the bending modulus is $k_b = 10^{-19}$ J; other parameters were held constant: $pK_a = 5$, $\Gamma = 1\ \mathrm{nm^{-2}}$, $\varepsilon = 80$, $T = 300$ K.

becomes thermodynamically preferable for the droplet to break up into small, nanoscale droplets as favored by electrostatic considerations alone. The size of these droplets decreases only weakly with increasing pH, as illustrated in Figure 3b (blue curve). These theoretical predictions are in qualitative agreement with the experimental trends (Figure 2).

Naturally, the thermodynamic arguments developed above cannot account for the existence of the metastable microemulsions prepared by lowering the pH of the nanodroplet phase. Because the droplets are negatively charged, they do not coalesce immediately but do so only over the course of several days. This kinetic stability can be understood qualitatively in terms of the Derjaguin–Landau–Verwey–Overbeek (DLVO) theory of colloidal stability, in which short-range attractions (typically, van der Waals forces) compete against longer-range electrostatic repulsions. Importantly, the surface potential of the droplets decreases with decreasing pH; for pH values lower than the pK_a value, the droplets aggregate rapidly.

With the ability to control droplet size, we considered the possibility of using our system to partition a "cargo" contained in the large droplet into the nanoscopic progeny micelles (Figure 4). As the cargo, we chose metal nanorods

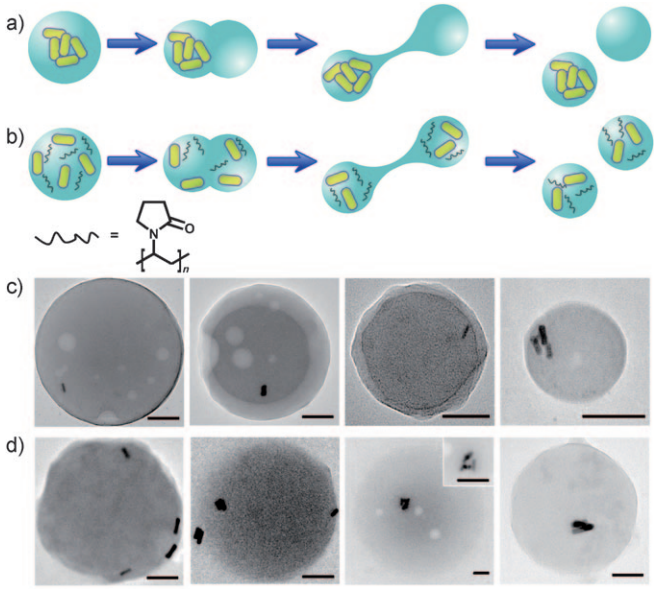

Figure 4. Self-dividing droplets partition nanoparticulate cargo (here, nanorods, NRs). a) In the absence of stabilizing PVP, the NRs aggregate, even as the droplets divide, while b) PVP helps to keep the nanorods separate, thus allowing them to partition evenly among the "daughter" droplets. c) Typical TEM images of the divided, (280 ± 22) nm inverse micelles at pH 12.3; each droplet contains, on average, 1.9 ± 1.0 NRs. d) TEM images of (350 ± 30) nm inverse micelles at pH 12 containing 4.9 ± 2.9 NRs per droplet. All scale bars correspond to 100 nm. TEM images were obtained by applying the inverse micelle solution onto an amorphous carbon-coated TEM grid and letting it evaporate. The bulk DCM organic phase evaporated rapidly, leaving behind water droplets that contain NRs, salt, and 2-HDA around the interface. Since the area of the droplets "flattened" on the substrate agreed with that estimated from DLS measurements of droplets in solution, it is reasonable to assume that coalescence of the droplets on the TEM grid was negligible.

(NRs, (41 ± 4.2) nm long, (10.5 ± 1.1) nm in cross-sectional diameter, see the Supporting Information), which can be readily imaged by TEM and, unlike spherical NPs, cannot be confused with impurities (see Figure S2 in the Supporting Information for typical images of NP-containing drops). The realization of this idea, however, required "inverting" the system from regular to reverse micelles with DCM/2-HDA solvent and basic water droplets.[18] The reason for doing so was that when the nanorods—even the ones functionalized with nonpolar *n*-alkane thiol ligands—were dispersed in an organic/nonpolar droplet phase at concentrations of approximately $10^{14}\ \mathrm{NR\,mL^{-1}}$, they tended to aggregate because of strong van der Waals attractions ($E_{vdw} \approx 18$ kT per side-by-side NR pair[19]), and these aggregates did not break up or divide when the droplets did. In contrast, the NRs stabilized with polar ligands such as mercaptoundecanoic acid, MUA

could be dispersed in aqueous droplets (Figure 4a). These droplets also contained 2% w/w of poly(vinyl pyrrolidone) (PVP), whose role was to prevent the aggregation of the NRs by steric-exclusion interactions[19] (the electrostatic repulsions between the NRs at high pH/high salt concentrations were screened and, by themselves, were too weak to keep the NRs dispersed).

The macroscopic droplets divided (Figure 4b) into nanomicelles at pH values above approximately 10. The inverted nanomicelles, however, were larger than those observed in the case of "normal" emulsions, because of the differences in the solution of the PB equation on the inside versus the outside of the droplets (see the Supporting Information for details). Importantly, the division process resulted in partitioning of the NRs approximately equally into the micelles. For example, micelles of an average diameter $d = (280 \pm 22)$ nm obtained at pH 12.3 each contained 1.9 ± 1.0 rods (Figure 4c) while $d = (350 \pm 30)$ nm micelles obtained at pH 12.0 had 4.9 ± 2.9 rods (droplet sizes determined by DLS; statistics for rods are based on the analysis of 13 TEM images for each condition). We note that these numbers agree with the initial concentration of the NRs (2×10^{14} NR mL^{-1}) based on which each micelle was predicted to contain 2.3 and 4.5 NRs, respectively. This result corroborates the assumption that the rods do not aggregate during division but rather partition in proportion to the volume of the droplet.

In summary, by partitioning the cargo they contain, self-dividing droplets can offer the advantages of both size control down to the nanoscale and also of speed (ca. 1 min for droplet division or "reverse" coalescence when $pH < pK_a$). These characteristics combined with the ability to partition the contents of the droplets suggest applications in dispersion and retrieval systems where the interfacial surface area would be first increased (e.g., to increase activity of heterogeneous catalysis by nanoparticles contained in the droplets) and then decreased (e.g., to retrieve the catalyst into one big droplet). Of course, development of such systems will require coupling of the "self-division" process with the interfacial chemistries that do not interfere with the surface-tension effects that mediate reversible emulsification.

Received: April 29, 2010
Published online: August 16, 2010

Keywords: interfaces · micelles · nanoparticles · self-reproduction · surfactants

[1] P. A. Bachmann, P. Walde, P. L. Luisi, J. Lang, *J. Am. Chem. Soc.* **1990**, *112*, 8200 – 8201.
[2] P. A. Bachmann, P. Walde, P. L. Luisi, J. Lang, *J. Am. Chem. Soc.* **1991**, *113*, 8204 – 8209.
[3] P. Walde, R. Wick, M. Fresta, A. Mangone, P. L. Luisi, *J. Am. Chem. Soc.* **1994**, *116*, 11649 – 11654.
[4] T. Oberholzer, R. Wick, P. L. Luisi, C. K. Biebricher, *Biochem. Biophys. Res. Commun.* **1995**, *207*, 250 – 257.
[5] M. M. Hanczyc, S. M. Fujikawa, J. W. Szostak, *Science* **2003**, *302*, 618 – 622.
[6] T. F. Zhu, J. W. Szostak, *J. Am. Chem. Soc.* **2009**, *131*, 5705 – 5713.
[7] T. Chou, M. V. Jaric, E. D. Siggia, *Biophys. J.* **1997**, *72*, 2042 – 2055.
[8] F. Jülicher, R. Lipowsky, *Phys. Rev. Lett.* **1993**, *70*, 2964 – 2967.
[9] R. Lipowsky, *Biophys. J.* **1993**, *64*, 1133 – 1138.
[10] I. Lagzi, S. Soh, P. J. Wesson, K. P. Browne, B. A. Grzybowski, *J. Am. Chem. Soc.* **2010**, *132*, 1198 – 1199.
[11] J. N. Israelachvili, *Intermolecular and Surface Forces*, Academic Press, San Diego, **1991**, p. 375.
[12] This treatment is similar to other soft matter systems in which the interplay between long-range electrostatic interactions and short-range attractive interactions are critical for the determination of both the domains and phases (Ref. [13]) and the stability (Ref. [14]) of the system.
[13] H. M. McConnell, L. K. Tamm, R. M. Weis, *Proc. Natl. Acad. Sci. USA* **1984**, *81*, 3249 – 3253.
[14] F. Cardinaux, A. Stradner, P. Schurtenberger, F. Sciortino, E. Zaccarelli, *Europhys. Lett.* **2007**, *77*, 48004.
[15] J. Amaya, D. Rana, V. Hornof, *J. Solution Chem.* **2002**, *31*, 139 – 148.
[16] H. Träuble, H. Eibl, *Proc. Natl. Acad. Sci. USA* **1974**, *71*, 214 – 219.
[17] D. Y. C. Chan, D. J. Mitchell, *J. Colloid Interface Sci.* **1983**, *95*, 193 – 197.
[18] Aqueous droplets containing NRs were prepared in the following manner: 6.0 mg poly(vinyl pyrrolidone) (PVP) was mixed with 150 μL NR solution and 150 μL of an aqueous tetramethylammonium hydroxide solution to give alkaline solutions of the desired pH. Immediately after mixing, 15 μL of this solution was added to 18 mL of toluene containing 5% (v/v) 2-HDA.
[19] K. J. M. Bishop, C. E. Wilmer, S. Soh, B. A. Grzybowski, *Small* **2009**, *5*, 1600 – 1630.

